Electric-Field Control of the Orbital Occupancy and Magnetic Moment of a Transition-Metal Oxide

Daniele Preziosi,* Marin Alexe, Dietrich Hesse, and Marco Salluzzo
Max Planck Institute of Microstructure Physics, Weinberg 2D-06120 Halle, Germany;
Department of Physics, University of Warwick, Coventry CV4 7AL, United Kingdom;
and CNR-SPIN, Complesso Universitario di Monte Sant'Angelo, via Cinthia I-80126 Napoli, Italy
(Received 10 November 2014; published 6 October 2015)

By using soft-x-ray linear and magnetic dichroism on $La_{0.825}Sr_{0.175}MnO_3/PbZr_{0.2}Ti_{0.8}O_3$ ferromagnetic-ferroelectric heterostructures we demonstrate a nonvolatile modulation of the Mn 3*d* orbital anisotropy and magnetic moment. X-ray absorption spectroscopy at the Mn $L_{2,3}$ edges shows that the ferroelectric polarization direction modifies the carrier density, the spin moment, and the orbital splitting of t_{2g} and e_g Mn 3*d* states. These results are consistent with polar distortions of the oxygen octahedra surrounding the Mn ions induced by the switching of the ferroelectric polarization.

DOI: 10.1103/PhysRevLett.115.157401 PACS numbers: 78.70.Dm, 75.70.Cn, 77.84.-s, 78.66.-w

Transition metal oxides (TMOs) have been widely studied in the last decades for the wide range of electronic properties and related intriguing physical phenomena, including colossal magnetoresistance in manganites [1,2] and high-T_c superconductivity in cuprates [3]. Because of strong electronic correlations, TMOs are characterized by ground states with entangled spin, charge, lattice, and orbital degrees of freedom [4]. As a consequence, these systems exhibit large sensitivity to strain, pressure, and chemical or electron doping [5]. Their electronic properties can be tuned by external stimuli, such as magnetic and electric fields, which can even induce phase transitions [6]. In the particular case of manganites [7], the related electronic and magnetic properties are strongly influenced by the orbital degrees of freedom [8]. The electronically active Mn 3*d* orbitals can be manipulated via static biaxial strain [9,10] or by interface-driven effects due to surface and interface symmetry breaking, as shown in the case of manganite ultrathin films [11]. The main challenge, however, is achieving an external and reversible control of the orbital polarization, a concept proposed in the past for a novel oxide based electronics, the so-called oxide *orbitronics* [12].

Recent scanning transmission electron microscopy measurements on manganite-ferroelectric heterostructures showed that the structure of the MnO_6 octahedra next to the interface depends on the direction of the ferroelectric polarization (P) [13]. Chen *et al.* interpreted these results as a signature of an inversion of the e_g Mn 3*d* orbital polarization (π_{orb}) and proposed the use of ferroelectric field effect devices (FEFEDs) for an electric-field control of the energy hierarchy of the Mn 3*d* orbitals. FEFEDs, working basically on an interface-driven effect [14], were already used to induce reversible electrostatic modification of the transport-magnetic properties of $La_{1-x}Sr_xMnO_3$ thin films [15–19]. However, up to now, a direct demonstration of a reversible electric-field control of the Mn 3*d* π_{orb} is still missing. In this Letter we report an electric-field control of the orbital occupancy and of the magnetic moment of $La_{0.825}Sr_{0.175}MnO_3$ (LSMO) thin films in FEFEDs based on $PbZr_{0.2}Ti_{0.8}O_3$ (PZT) ferroelectric layers characterized by a long retention time (see Fig. S1 of the Supplemental Material [20] for details). We used x-ray absorption spectroscopy (XAS), linear, and magnetic circular dichroism (XLD, XMCD) measurements to investigate the effect of the P switching on the Mn 3*d* orbital anisotropy and on the magnetic moment of patterned LSMO(6 nm)/PZT(60 nm)/LSMO(12 nm) heterostructures. XAS under electric field application was used in the past to study the mechanism of the field effect doping field in high-T_c cuprate thin films [21].

XAS measurements were performed at the Soleil synchrotron radiation facility at the beam line Deimos [22]. Figure 1(a) shows an optical image of the FEFED used for the XAS experiments, which is composed by two back-gated 200×100 μm^2 Hall-bar channels (see also Fig. S3 of the Supplemental Material [20]). The PZT layers lying underneath the channel area were switched by applying a suitable sequence of voltage pulses between the bottom (gate) and top (HB) LSMO layers. The switching was performed *ex situ* for both FEFEDs engineered on the same heterostructure and, for each switching cycle, the two FEFEDs were settled in a P state opposite to each other. To verify the effect of the P reversal on the same FEFED in the spectroscopy properties, both FEFEDs were measured also after a second and a third switching experiment [see Figs. S4(a),(b),(c) of the Supplemental Material [20]].

In Fig. 2 we show the effect of the P reversal on the Mn L_3-edge isoXAS spectra, i.e., $(2I_{ab} + I_c)$, acquired at room temperature. We observed pronounced spectral changes by switching P, consisting in a shift of the Mn L_3 absorption peak and in a modification of the multiplet structure. In particular, the main L_3 peak moves towards lower (higher)

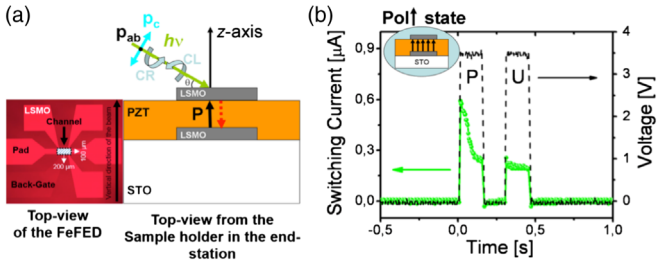

FIG. 1 (color online). (a) (Left side) Top-view optical image of the FEFED clearly indicating the channel and Pad area of the Hall bar geometry. (Right side) Schematic view of the XAS experiment on the LSMO/PZT/LSMO FEFED. The photon linear polarizations can be set parallel (p_{ab}) or almost perpendicular to the ab plane (p_c) and, the intensity of the related XAS spectra are labeled as I_{ab} and I_c, respectively. CR and CL indicate photons circularly right and left polarized, respectively. (b) Ferroelectric switching of the PZT layer with positive voltage pulses P and U, corresponding to the Pol↑ state (P pointing toward the top LSMO layer, see inset).

energy in the Pol↑ (Pol↓) state. The effect is consistent with a decrease or increase of the average Mn oxidation in the holes-depletion or holes-accumulation states, which manifest in a decrease or increase of the average Mn oxidation. The latter is due to the change of the Mn^{4+} fraction, which is characterized by $L_{2,3}$ peaks theoretically shifted to higher energy with respect to the Mn^{3+} ones. To have a rough estimation of the average electrostatic doping modulation, we compare the energy shift of the main features of the isoXAS spectra as a function of P with reference data acquired on $La_{1-x}Sr_xMnO_3$ thin films characterized by different x (see Fig. S5 of the Supplemental Material [20] for details). We find an overall modulation of (0.045 ± 0.007) holes/Mn due to the P reversal. Since the x-ray probing depth (of the order of 7.5 nm [23]) is

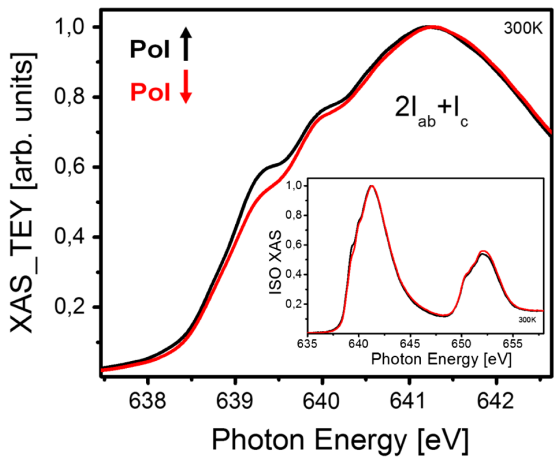

FIG. 2 (color online). Mn L_3-edge isoXAS spectra measured at room temperature for both Pol↓ (red line) and Pol↑ (black line) states. The inset shows the complete energy dependence of the isoXAS spectra.

larger than the LSMO thickness and P is expected to affect only the interfacial LSMO unit cells, the effective change in the carrier density of the region next to the PZT is expected to be even larger. These data are in qualitative agreement with the spectral changes observed at the O-K edge, as shown in the Supplemental Material [20] (Fig. S7).

The magnetic properties of the LSMO channel at 4.2 K are also modulated by the P reversal as demonstrated by the Mn $L_{2,3}$-edges XMCD spectra (see Fig. S6 of the Supplemental Material [20] file). In Table I we list the orbital (m_{orb}), effective spin ($m_{\mathrm{spin}}^{\mathrm{eff}}$) and corrected spin ($m_{\mathrm{spin}}$) moments obtained from the XMCD sum rules. We find that m_{orb} is close to zero for both P states due to the quenching of the orbital moment by the crystal field. However, the spin moment depends on the P direction and, in both saturation and remnant states, it is higher in the Pol↑, i.e., the hole-depletion state. This result is the expected one since the total magnetic moment in manganites follows the relation $(4\text{-}x)\mu_B/\mathrm{Mn}$, where x is the fraction of Mn^{4+} in the system which is higher in the Pol↓ (hole accumulation). The observed trend is in agreement also with results reported in the literature [15,19]. It is important to underline that the XMCD sum rules are not exact for the Mn edge. However, the changes as a function of P, at least qualitatively, are correct.

The key result of this work it is the direct demonstration of the modulation of the Mn-3d π_{orb} (i.e., change of the orbital occupancy and relative energy splitting) via P reversal as shown in Figs. 3 and 4 for the Pol↓ and Pol↑ states, respectively. By a simple comparison of the two XLD spectra defined as the difference $I_{ab} - I_c$ [with reference to Fig. 1(a)], one can infer a strong effect of the P direction on the π_{orb}. In particular, the tails at ~640 eV of the L_3 peaks extend to negative values in the Pol↓ state (see red line in Fig. 3), while they almost disappear in the Pol↑ state (see black line in Fig. 4). In order to determine the degree of the Mn 3d π_{orb} for both P states, we used the linear dichroism sum rules. The integrated XLD spectra normalized to the integrated total absorption D_L is related to π_{orb} through the equation

TABLE I. m_{orb}, $m_{\mathrm{spin}}^{\mathrm{eff}}$, and m_{spin} values (μ_B/Mn) as obtained from the application of the sum rules [24,25] to the XMCD spectra acquired at 4.2 K in grazing incidence conditions (H applied almost parallel to the device plane), for both P states. Following Ref. [26], we used a correction of 50% giving a good agreement between the spin moment obtained through XMCD and SQUID magnetometer measurements for LSMO ($x = 0.3$) thin films.

$\mu_o H$(T)	Pol↑ 0	Pol↑ 5	Pol↓ 0	Pol↓ 5
m_{orb}	< 0.005	< 0.005	0.015	0.045
$m_{\mathrm{spin}}^{\mathrm{eff}}$	1.03	1.8	0.75	1.49
m_{spin}	2.06	3.6	1.5	2.98

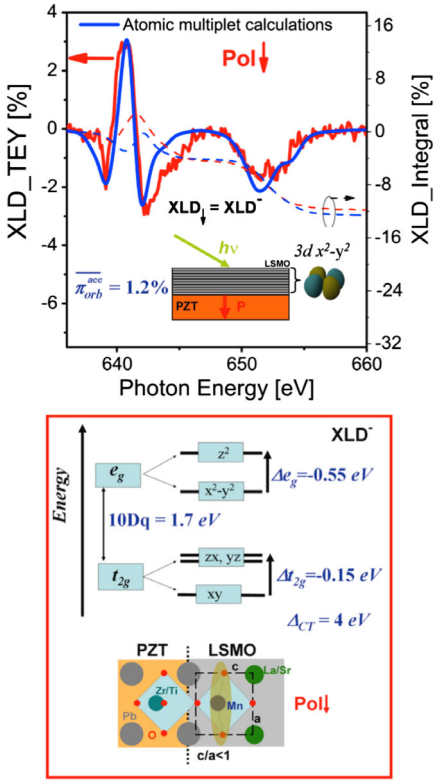

FIG. 3 (color online). Comparison between the atomic multiplet calculations (solid blue lines) and the experimental XLD spectra described in the text for the Pol↓ state. The dotted lines represent the integration curves calculated from the XLD spectrum and the related simulation. The inset in the upper panel sketches π_{orb} as a function of the P direction. In the lower panel the energy diagram is related to the XLD^{-} fitting parameters. The schematic ionic model, used to justify the modulation of the orbital occupancy has been re-adapted from Ref. [13]. XAS spectra were measured at 300 K in order to exclude any possible magnetic contribution.

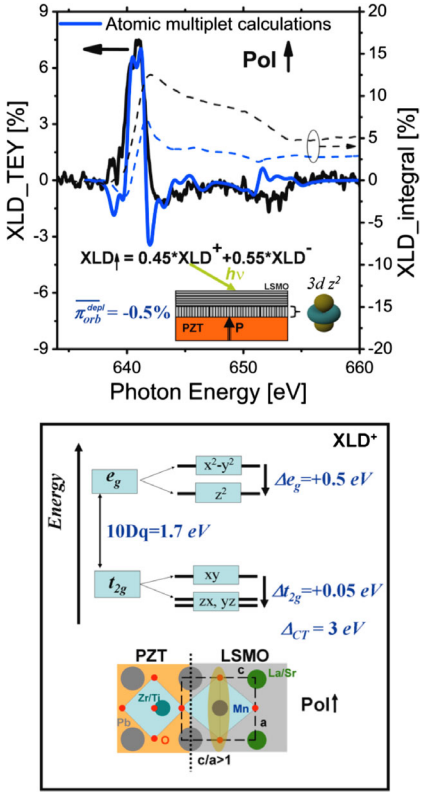

FIG. 4 (color online). Same as in Fig. 3 but related to the Pol↑ state.

$$D_L = \frac{\int_{L_3+L_2}(I_{ab}-I_c)dE}{\int_{L_3+L_2}(2I_{ab}+I_c)dE} \simeq \frac{1}{2}\frac{n_{z^2}-n_{x^2-y^2}}{n_{z^2}+n_{x^2-y^2}} = -\frac{1}{2}\pi_{\mathrm{orb}}, \quad (1)$$

where $n_{x^2-y^2}$ and n_{z^2} are the electron occupancy in the e_g $3d_{x^2-y^2}$ and $3d_{z^2}$ orbitals, respectively. π_{orb} is defined as in Ref. [13]. The integration curves of the experimental XLD spectra for each P state are shown as red and black dotted lines in Figs. 3 and 4, respectively. Notably, D_L is negative in the Pol↓ state and positive in the Pol↑ state. According to Eq. (1) a preferential electron occupancy of the in-plane $3d_{x^2-y^2}$ orbitals is favored in the Pol↓, while the occupancy of out-of-plane $3d_{z^2}$ ones is favored in the Pol↑ state. The data correspond to a change of the average polarization of the e_g orbitals from $+1.2\%$ (Pol↓ state) to -0.5% (Pol↑ state), showing that the energy hierarchy of the Mn $3d$ states is controlled via P switching. In order to get more information on the changes of the electronic properties of the LSMO layer as a function of P, we performed multiplet splitting calculations to simulate the observed XLD data [27]. Because of the low level of chemical doping of the LSMO layer, i.e., $x = 0.175$, we assumed a Mn^{3+} configuration for the Mn ions in D_{4h} symmetry, a crystal field $10Dq$ of 1.7 eV, and a nonzero splitting of the in-plane and out-of-plane Mn $3d$ t_{2g} and e_g orbitals, i.e., $\Delta t_{2g} = E_{xy}$-$E_{xz,yz}$ and $\Delta e_g = E_{x^2-y^2}$-E_{z^2}. The partially covalent nature of the Mn $3d$—O $2p$ bonding was modeled in the calculation by charge transfer (CT) effects parametrized by the charge transfer energy Δ_{CT} and by the difference between the Coulomb energy associated to the core-hole interaction U_{pd} and the U_{dd} Hubbard potential, i.e., U_{pd}-$U_{dd} = 1.5$ eV [28]. The XLD spectrum obtained in the Pol↓ state ($\mathrm{XLD}_{\downarrow}$) is reasonably reproduced by assuming an homogeneous electronic state for the whole LSMO film, as shown by the solid blue line of Fig. 3 obtained with fitting parameters $\Delta t_{2g} = -0.15$, $\Delta e_g = -0.55$, and Δ_{CT} of 4 eV. The set of parameters that simulates at best the $\mathrm{XLD}_{\downarrow}$ spectrum is designed as XLD^{-}, while the corresponding energy diagram is shown in the bottom panel of Fig. 3. Interestingly, a similar XLD spectrum is also obtained in areas of the upper LSMO layer *outside the channel*, i.e., the pads, which cannot be switched (no gate electrode). This result confirms that the as-grown P state of the FEFEDs is Pol↓ (P pointing away from the upper LSMO layer). This P direction determines

a structural or orbital effect which mainly induces a preferential occupancy of the in-plane $3d_{x^2-y^2}$ orbitals.

The XLD spectra in the Pol↑ state (i.e., $XLD_{\uparrow}$), on the other hand, cannot be explained assuming a uniform π_{orb} in the whole LSMO thickness. Indeed, the $XLD_{\uparrow}$ spectrum, while showing a much reduced negative tail at the L_3 peak (which, basically, determines the negative sign of D_L for $XLD_{\downarrow}$), is still characterized by a positive peak at L_3 and a reduced, but negative, feature at the L_2. In this case we should make the simple and reasonable assumption that only the interfacial LSMO unit cells are affected by the P reversal. As a result, the LSMO channel is modeled as constituted by two parts (whose relative thickness is a fitting parameter of the model), as schematically illustrated in the sketch of Fig. 4 (upper panel): the top-most unit cells of the LSMO layer, not affected by the P reversal, steadily characterized by the same set of parameters (XLD^{-}, fitting $XLD_{\downarrow}$); and the interfacial unit cells, which are affected by the P switching. Interestingly, the best agreement between the $XLD_{\uparrow}$ spectrum along with its integral (sign and shape) and the calculations (see solid and dotted blue lines in the upper panel of Fig. 4) is obtained assuming that the Mn $3d$ energy hierarchy of the interfacial unit cells is fully reversed in the Pol↑ state ($\Delta t_{2g} = +0.05$, $\Delta e_g = +0.5$, and Δ_{CT} of 3 eV) and that they contribute to the total $XLD_{\uparrow}$ by a fraction of 45% of the total signal. The set of parameters that account for this interfacial contribution to the overall $XLD_{\uparrow}$ spectrum is designed as XLD^{+}, while the corresponding energy diagram is shown in the bottom panel of Fig. 4. Thus a preferential out-of-plane occupancy of the Mn $3d$ orbitals of the interfacial unit cells is realized for the Pol↑ state. Taking into account the different contributions to $XLD_{\uparrow}$ from the interfacial and top-most unit cells, we estimate that the thickness of the LSMO layer affected by the P switching is ~2.7 nm. It is worth noting that heterostructures with a LSMO channel of only 2.5 nm in thickness and, characterized by a Pol↑ state for the as-grown PZT polarization, show a full $3d_{z^2}$ electron occupation, in agreement with our finding (see Fig. S11 in the Supplemental Material [20]) [29].

The analysis of the Mn $L_{2,3}$-edges XLD spectra is qualitatively confirmed by O K-edge XLD data (details are in Fig. S8 of the Supplemental Material [20]), showing that the P reversal gives rise to the emergence of a $3d_{z^2}$ electron occupation component, very similar to the one observed in the case of LSMO films deposited on $LaAlO_3$ substrates [9].

The experimental data can be explained by taking into account the P-dependent structural distortion of the interfacial MnO_6 octahedra [13]. Because of the presence of an electric field, the oxygen ions and the cations move in opposite directions along the interface normal, determining a substantial alteration of the out-of-plane Mn-O distance and of the Mn-O in-plane angle (rumpling), as shown schematically in the lower panel of Figs. 3 and 4 for both P states. Precisely, for the Pol↓ state the MnO_6 octahedra are substantially compressed along the c direction, so that $c/a < 1$. Moreover, the Mn-O bonding is not straight and forms an angle lower than 180°. As a result, a preferential in-plane occupancy of the e_g orbitals is favored as demonstrated by the value and sign of D_L in the Pol↓ state. On the other hand, in the Pol↑ state, a clear π_{orb} inversion takes place, corresponding to a preferential occupancy of the out-of-plane e_g orbitals. In this case, the MnO_6 octahedra become substantially elongated along the c direction (i.e., $c/a > 1$), with a subsequent preferential $3d_{z^2}$ orbital occupancy, in line with *ab initio* calculations presented in Ref. [13]. A more quantitative comparison between experiments and the theoretical model of Ref. [13] would require layer resolved XLD measurements. However, the average Mn π_{orb} value that we find is in reasonable agreement, in terms of magnitude and sign, with the theoretical results averaged over the first 8 interfacial unit cells.

Our results demonstrate that an electric-field control of transition metals orbital polarization can be achieved at room temperature using a FEFED. The latter introduces, in the panorama of the orbital physics, a novel and simple approach to tune the electronic and, eventually the magnetic properties, of a TMO. Hence, the P reversal not only modulates the carrier density but also the orbital degrees of freedom. Along this direction, the engineering of FEFEDs constituted by ultrathin TMO (i.e., manganite) layers, still demonstrating proper functional properties (e.g., ferromagnetism and orbital orders), would be of extreme relevance. Furthermore, a control over the orbital degrees of freedom can open several opportunities not limited to manganites and TMO materials. For example, by tuning the orbital anisotropy, an inversion of the $3d$ bands can be achieved at the surface and interface of materials characterized by non-negligible spin-orbit coupling, offering the possibility to create (or destroy) topological states. Candidates are iridate [30] based heterostructures and transition metal dicalcogenides [31].

We acknowledge SOLEIL synchrotron for provision of synchrotron radiation facilities at beam line DEIMOS (Proposal No. 20130820). D. P. thanks the European Community's Seventh Framework Programme (FP7/2007-2013) for financial support under Grant Agreement No. NMP3-LA-2010-246102.

*Present address: Unité mixte de physique CNRS/Thales, campus de l'École polytechnique, 1, avenue Augustin-Fresnel, 91767 Palaiseau, France.
daniele.preziosi@thalesgroup.com

[1] M. Salamon and M. Jaime, Rev. Mod. Phys. **73**, 583 (2001).
[2] K. Dörr, J. Phys. D **39**, R125 (2006).
[3] E. Fradkin and S. Kivelson, Nat. Phys. **8**, 864 (2012).
[4] E. Dagotto, Science **309**, 257 (2005).

[5] M. Imada, A. Fujimori, and Y. Tokura, Rev. Mod. Phys. **70**, 1039 (1998).
[6] C. H. Ahn, J. Triscone, and J. Mannhart, Nature (London) **424**, 1015 (2003).
[7] J. Coey, M. Viret, and S. von Molnar, Adv. Phys. **48**, 167 (1999).
[8] Y. Tokura and N. Nagaosa, Science **288**, 462 (2000).
[9] C. Aruta, G. Ghiringhelli, A. Tebano, N. Boggio, and N. Brookes, Phys. Rev. B **73**, 235121 (2006).
[10] A. Tebano, C. Aruta, S. Sanna, P. G. Medaglia, G. Balestrino, A. A. Sidorenko, R. De Renzi, G. Ghiringhelli, L. Braicovich, V. Bisogni, and N. B. Brookes, Phys. Rev. Lett. **100**, 137401 (2008).
[11] D. Pesquera, G. Herranz, A. Barla, E. Pellegrin, F. Bondino, E. Magnano, F. Snchez, and J. Fontcuberta, Nat. Commun. **3**, 1189 (2012).
[12] B. A. Bernevig, T. L. Hughes, and S.-C. Zhang, Phys. Rev. Lett. **95**, 066601(2005).
[13] H. Chen, Q. Qiao, M. S. J. Marshall, A. B. Georgescu, A. Gulec, P. J. Phillips, R. F. Klie, F. J. Walker, C. H. Ahn, and S. Ismail-Beigi, Nano Lett. **14**, 4965 (2014).
[14] X. Hong, A. Posadas, and C. H. Ahn, Appl. Phys. Lett. **86**, 142501 (2005).
[15] H. J. A. Molegraaf, J. Hoffman, and S. Gariglio, Adv. Mater. **21**, 3470 (2009).
[16] C. A. F. Vaz, Y. Segal, J. Hoffman, R. D. Grober, and F. J. Walker, Appl. Phys. Lett. **97**, 042506 (2010).
[17] C. A. F. Vaz, J. Hoffman, C. Ahn, and R. Ramesh, Adv. Mater. **22**, 2900 (2010).
[18] C. A. F. Vaz, J. Hoffman, Y. Segal, J. W. Reiner, R. D. Grober, Z. Zhang, C. H. Ahn, and F. J. Walker, Phys. Rev. Lett. **104**, 127202 (2010).
[19] D. Preziosi, I. Fina, E. Pippel, D. Hesse, X. Marti, F. Bern, M. Ziese, and M. Alexe, Phys. Rev. B **90**, 125155 (2014).
[20] See Supplemental Material at http://link.aps.org/supplemental/10.1103/PhysRevLett.115.157401 for additional data concerning this Letter.
[21] M. Salluzzo, G. Ghiringhelli, J. C. Cezar, N. B. Brookes, G. M. DeLuca, F. Fracassi, and R. Vaglio, Phys. Rev. Lett. **100**, 056810 (2008).
[22] P. Ohresser, E. Otero, F. Choueikani, K. Chen, S. Stanescu, F. Deschamps, T. Moreno, F. Polack, B. Lagarde, B. Muller, F. Marteau, F. Scheurer, L. Joly, O. Bunau, and P. Sainctavit, Rev. Sci. Instrum. **85**, 013106 (2014).
[23] B. Frazer, B. Gilbert, B. Sonderegger, and G. D. Stasio, Surf. Sci. **537**, 161 (2003).
[24] C. T. Chen, Y. U. Idzerda, H. J. Lin, N. V. Smith, G. Meigs, E. Chaban, G. H. Ho, E. Pellegrin, and F. Sette, Phys. Rev. Lett. **75**, 152 (1995).
[25] C. Dallera, *Resonant Spectroscopies with Synchrotron Radiation*, Cours du Troisième Cycle (Ecole Polytechnique Fédérale de Lausanne, Switzerland, 2003).
[26] C. Piamonteze, P. Miedema, and F. M. F. de Groot, Phys. Rev. B **80**, 184410 (2009).
[27] E. Stavitski and F. M. F. de Groot, Micron **41**, 687 (2010).
[28] F. de Groot, J. Electron Spectrosc. Relat. Phenom. **62**, 111 (1993).
[29] Unfortunately those devices were not switchable due to the too insulating character of the thin LSMO layer.
[30] C. Lu, S. Dong, A. Quindeau, D. Preziosi, N. Hu, and M. Alexe, Phys. Rev. B **91**, 104401 (2015).
[31] H. Yuan, M. Bahramy, K. Morimoto, S. Wu, and K. Nomura, Nat. Phys. **9**, 563 (2013).